Lithos 366–367 (2020) 105575

Contents lists available at ScienceDirect

Lithos

journal homepage: www.elsevier.com/locate/lithos

Research Article

Petrogenesis of Late Carboniferous A-type granites and Early Cretaceous adakites of the Songnen Block, NE China: Implications for the geodynamic evolution of the Paleo-Asian and Paleo-Pacific oceans

Guozhan Xu [a,b], Changzhou Deng [a,*], Chenglu Li [a,b,*], Changlu Lv [a,b], Runsheng Yin [a], Jishuang Ding [a,b], Maowen Yuan [c], Jun Gou [d]

[a] State Key Laboratory of Ore Deposit Geochemistry, Institute of Geochemistry, Chinese Academy of Sciences, Guiyang 550081, China
[b] Heilongjiang Institute of Geological Survey, Harbin 150036, China
[c] State Key Laboratory of Geological Processes and Mineral Resources, Institute of Earth Sciences, China University of Geosciences, 100083 Beijing, China
[d] College of Earth Sciences, Jilin University, Changchun 130061, China

ARTICLE INFO

Article history:
Received 25 October 2019
Accepted 8 May 2020
Available online xxxx

Keywords:
A-type granites
Adakites
Petrogenesis
Paleo-Asian Ocean
Paleo-Pacific flat slab

ABSTRACT

The petrogenesis of Late Carboniferous A-type granites and Early Cretaceous adakites in NE China offers new insights into the geodynamic evolution of the Paleo-Asian and Paleo-Pacific oceans. This study reports new LA–ICP–MS zircon U—Pb ages, geochemical data, and zircon Hf isotopic compositions of syenogranites and quartz diorite porphyries exposed on the northern margin of the Songnen Block, NE China. Zircon U—Pb age data indicate that the syenogranites and quartz diorite porphyries were emplaced at ca. 319 and 120 Ma, respectively. The syenogranites have high K_2O contents of 4.15–4.79 wt% and (K_2O + Na_2O)/CaO ratios of 33–102, and low MgO (0.06–0.20 wt%) and P_2O_5 (0.01–0.02 wt%) contents. Their remarkably high HREE contents and Y/Nb ratios (2.07–2.40), significantly negative Eu anomalies ($Eu/Eu^* = 0.15–0.28$), and low Sr contents (29.7–85.8 ppm) indicate that the syenogranites are A-type granites. They have positive zircon $\varepsilon_{Hf}(t)$ values of 8.4–12.1 and Neoproterozoic Hf T_{DM2} ages of 795–561 Ma, suggesting a juvenile lower crustal source. The quartz diorite porphyries have relatively high Na_2O and MgO, and moderate K_2O contents. Their A/CNK values (0.95–1.18) indicate a transition from being metaluminous to weakly peraluminous. They are enriched in LILEs (e.g., Rb, K, and Ba) and depleted in HFSEs (e.g., Nb, Ta, Ti, and P). Their low Y (11.1–14.4 ppm) and Yb (0.98–1.34 ppm) contents and high Sr (589–1131 ppm), Cr, and Ni contents and Sr/Y ratios indicate that they were generated by partial melting of oceanic crust. Based on these data and regional geological investigations, we propose that the syenogranites on the northern margin of the Songnen Block were formed in a post-collision extensional setting, likely due to closure of the Paleo-Asian Ocean between the Xing'an and Songnen blocks. Formation of the Early Cretaceous quartz diorite porphyries may have been triggered by partial melting of the Paleo-Pacific flat slab. Apart from rollback of the Paleo-Pacific oceanic slab, the main reason for the eastward migration of magmatism during the Cretaceous was the trench-ward dehydration, eclogitization, and sinking of the residual Paleo-Pacific flat slab.

1. Introduction

The geological setting of NE China was characterized by multistage subduction of the Paleo-Asian, Paleo-Pacific, and Mongol–Okhotsk oceanic plates (Deng et al., 2019; Sun et al., 2013; Tang et al., 2014; Wu et al., 2011; Xu et al., 2015) and amalgamation of the Erguan, Xing'an, Songnen, and Jiamusi blocks during the Phanerozoic (Fig. 1a–b; Sengör et al., 1993; Ge et al., 2005; Xu et al., 2013; Zhou et al., 2018). Studies of the widespread igneous rocks in NE China provide valuable insights into the geodynamic evolution of both the Paleo-Asian and Paleo-Pacific oceans within the same overlying plate (e.g., Ji et al., 2019; Wang et al., 2019; Wu et al., 2011; Zhou et al., 2018). Previous studies proposed that the Paleo-Asian Ocean closed during the late Permian–Early Triassic along the South Tianshan–Beishan–Xar Moron–Changhun Suture Zone (Sengör et al., 2018; Xiao et al., 2015; Xu et al., 2015; Zhou et al., 2018; Zhou and Wilde, 2013). However, the timing of its final closure between the Songnen and Xing'an blocks is still debated, with proposals including the Paleozoic (e.g., ca. 400 Ma, Xu et al., 2015; ca. 383 Ma, Xu et al., 2001; ca. 351 Ma, Li et al., 2013; ca. 333 Ma, Zhou et al., 2005), before the early Permian

* Corresponding authors at: State Key Laboratory of Ore Deposit Geochemistry, Institute of Geochemistry, Chinese Academy of Sciences, Guiyang 550081, China.
E-mail addresses: changzhouhn@126.com (C. Deng), lcl230881@163.com (C. Li).

https://doi.org/10.1016/j.lithos.2020.105575
0024-4937/

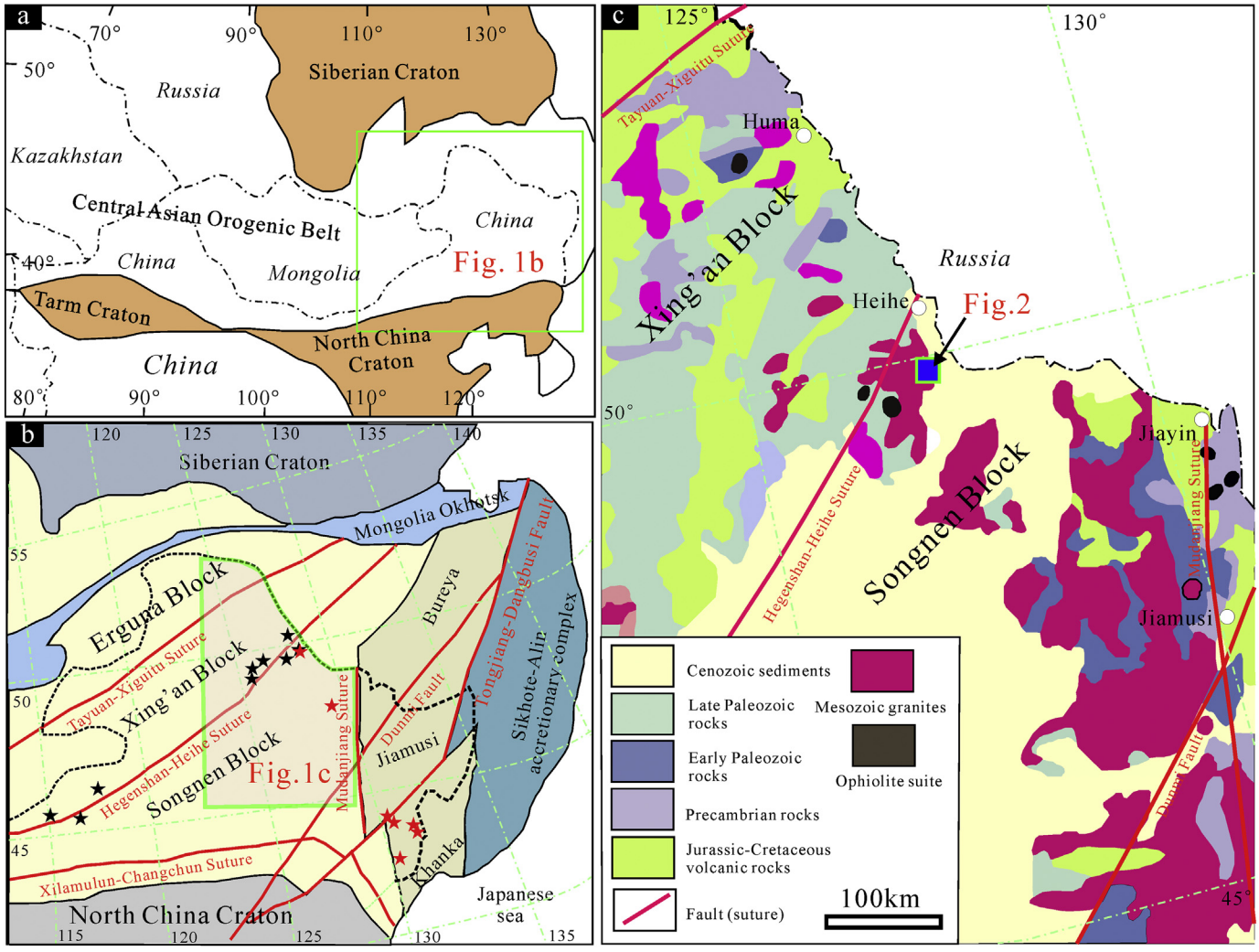

Fig. 1. (a) Tectonic map showing the Central Asian Orogenic Belt (after Jahn, 2004). (b) Geological map of NE China (modified from Wu et al., 2007), showing the locations of Late Carboniferous–early Permian A-type granites (black stars; after Zhang et al., 2013) and Early Cretaceous adakites (red stars; after Wang et al., 2019). (c) Simplified geological map of the eastern Xing'an and Songnen blocks (after Chen et al., 2017a). (For interpretation of the references to colour in this figure legend, the reader is referred to the web version of this article.)

(Tong et al., 2015; Zhang et al., 2015; Ma et al., 2019; based on a study of Permian A-type granites in NE China and adjacent areas), or early Mesozoic (Miao et al., 2003). The northwestward subduction of the Paleo-Pacific Plate beneath Eurasia during the late Mesozoic has been described in terms of flat slab subduction during the Late Jurassic (Ji et al., 2019; Kiminami and Imaoka, 2013), with slab rollback during the late Early–Late Cretaceous causing steep subduction (Ji et al., 2019; Ouyang et al., 2013; Wang et al., 2019). However, the switch of Paleo-Pacific Plate subduction from flat to steep, which may be important in explaining propagation of the late Mesozoic volcanic belt far into the interior of NE China, remains poorly constrained.

A-type and adakitic granitoids are increasingly being reported in NE China (Fig. 1b; Zhang et al., 2013; Li et al., 2014; Deng et al., 2018a; Wang et al., 2019), with previous studies indicating that Late Carboniferous–early Permian A-type granites are mainly distributed along the Hegenshan–Heihe Suture Zone (Li et al., 2014; Ma et al., 2019; Tong et al., 2015; Wu et al., 2002; Zhang et al., 2013; Zhang et al., 2015). These A-type granites serve as a temporal magmatic milestone in the amalgamation of the Songnen and Xing'an blocks, and improve our understanding of the tectonic evolution in the eastern Central Asian Orogenic Belt (CAOB; Wu et al., 2002; Li et al., 2014; Tong et al., 2015; Zhang et al., 2015; Ma et al., 2019). Cretaceous adakitic rocks have mainly been discovered in eastern NE China, and are suggested to have been generated by subduction of the Paleo-Pacific Plate beneath Eurasia (Ji et al., 2019; Wang et al., 2019; Zhao et al., 2012). Previous studies have shown that A-type granites are generally formed in an extensional setting (Eby, 1992; Sylvester, 1998), while adakites have a convergent margin affinity (Sun et al., 2011, 2012). Studies of the petrogenesis of Late Carboniferous A-type granites and Early Cretaceous adakites may thus provide new insights into the geodynamic evolution of NE China during the Late Carboniferous and Early Cretaceous.

Here we present new zircon U—Pb ages, whole-rock geochemical data, and zircon Hf isotopic compositions for A-type granites and adakites in the northeastern Songnen Block, NE China (Fig. 1c). We constrain the petrogenesis of the studied rocks and discuss the geodynamic evolution of the Paleo-Asian and Paleo-Pacific oceans.

2. Geological setting and sample descriptions

The Songnen Block lies in the eastern CAOB, bordered by the Jiamusi Block along the Jiamusi Suture Zone to the southeast, and connecting with the Xing'an Block along the Hegenshan–Heihe Suture Zone to the northwest (Fig. 1). Tectonism, magmatic activity, and crustal accretion in the Songnen Block were mainly controlled by the evolution of the

Paleo-Asian Ocean during the Paleozoic–early Mesozoic and the Paleo-Pacific Ocean during the late Mesozoic (Wu et al., 2011; Xu et al., 2013). A series of N—S—, NE–SW-, NW–SE-, and E–W-trending faults, which provided favorable conditions for the generation of igneous rocks and polymetallic deposits (Chen et al., 2017b), developed in the Songnen Block through complex tectonic processes. The Precambrian crystalline basement of the Songnen Block comprises predominantly the Proterozoic Dongfengshan and Zhangguangcailing groups, which are dominated by marble, phyllite, mica schist, sericite–quartz schist, amphibolite, biotite granulite–gneiss, and granulite, with a few areas of these rocks being exposed in the northern block (Xu et al., 2015; Yang et al., 2012; Zhou et al., 2018). Paleozoic strata in the Songnen Block were formed during the Cambrian, Ordovician, and Permian, and comprise mainly marine sedimentary strata that were associated with intense magmatism and deformation, and are intruded by large volumes of Late Triassic–Early Jurassic coarse-grained granites (Wu et al., 2011). Mesozoic strata are dominated by voluminous Early Jurassic basalt, trachyandesite, andesite, and rhyolite, with minor Triassic and Jurassic fluvial and lacustrine deposits (Xu et al., 2013). In addition to the widely distributed I- and A-type Late Triassic–Early Jurassic granites, there are intrusive rocks in the form of batholiths and stocks comprising Early Cretaceous granites, and minor A-type Paleozoic and I-type early Mesozoic granites (Deng et al., 2018a; Liu et al., 2008; Zhang et al., 2013).

The studied Late Carboniferous syenogranites and Early Cretaceous quartz diorite porphyries are from the southern Heihe area in the northeastern Songnen Block (Fig. 1c). The syenogranites generally occur as batholiths covered partially by the upper Permian Wudaoling Formation comprising mainly andesites and rhyolites, and the Lower Cretaceous Tamulangou Formation comprising mainly basaltic andesites, trachyandesites, andesites, and breccias with calc-alkaline affinities (HBGMR, 1997). The quartz diorite porphyries are distributed in the northern part of the study area. This gray porphyritic rock intrudes the syenogranites and upper Permian Wudaoling Formation as stocks and veins (Fig. 2).

Outcrops of the syenogranites have gray weathered and red fresh surfaces (Fig. 3). The syenogranites have medium-grained textures (Fig. 3a–c) and comprise mainly quartz (25–30 vol%), perthite (20–25 vol%), orthoclase (20–30 vol%), biotite (3–5 vol%), and plagioclase (5–10 vol%), with accessory minerals including titanite, zircon, and apatite. The quartz diorite porphyries are massive in structure and porphyritic in texture with a microgranular groundmass (Fig. 3d–f). Phenocrysts in the quartz diorite porphyries make up ~40 vol% of the rocks, including 20–30 vol% medium–fine-grained plagioclase, 10–15 vol% medium-grained biotite, and sparse hornblende.

3. Analytical methods

3.1. Zircon U—Pb dating

Samples of two syenogranites (samples BQH-9 and BQH-11) and two quartz diorite porphyries (BQH-1 and BQH-5) were chosen for

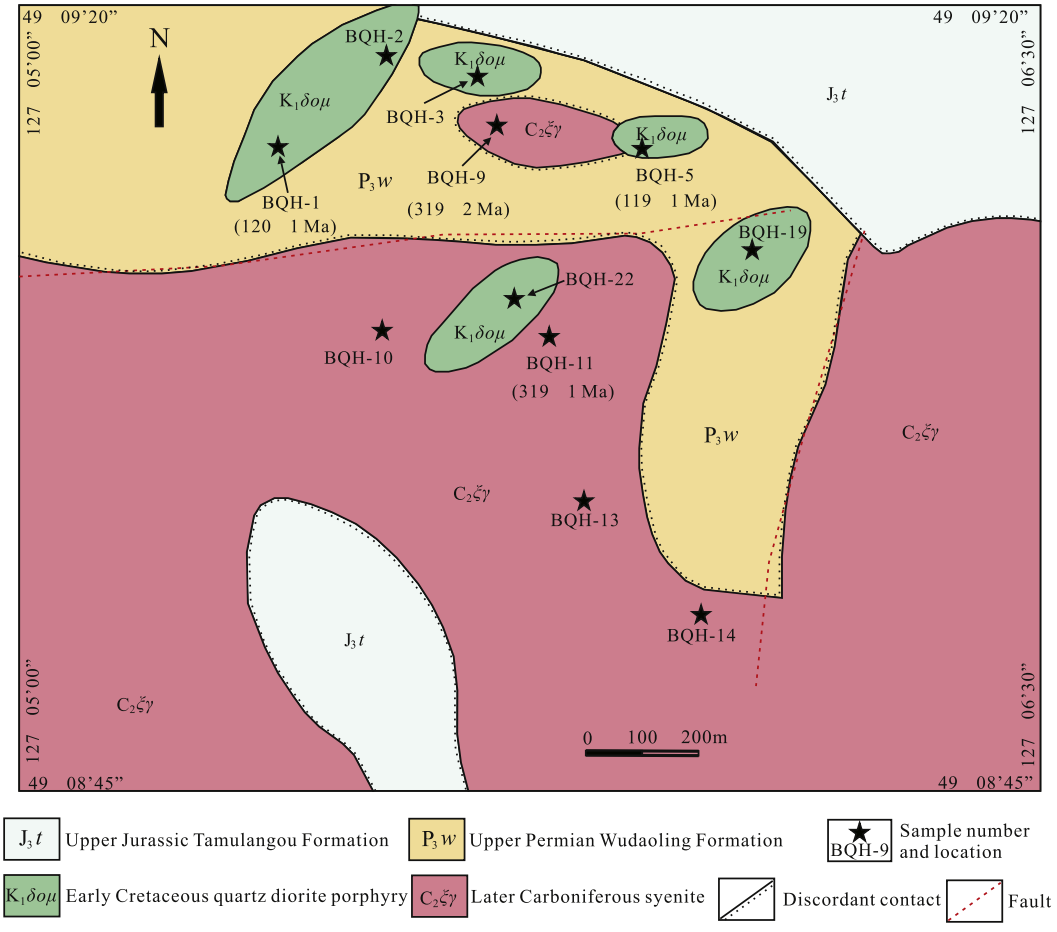

Fig. 2. Geological map of the northeastern Songnen Block, showing the distribution of Late Carboniferous syenogranites and Early Cretaceous quartz diorite porphyries, with sample locations.

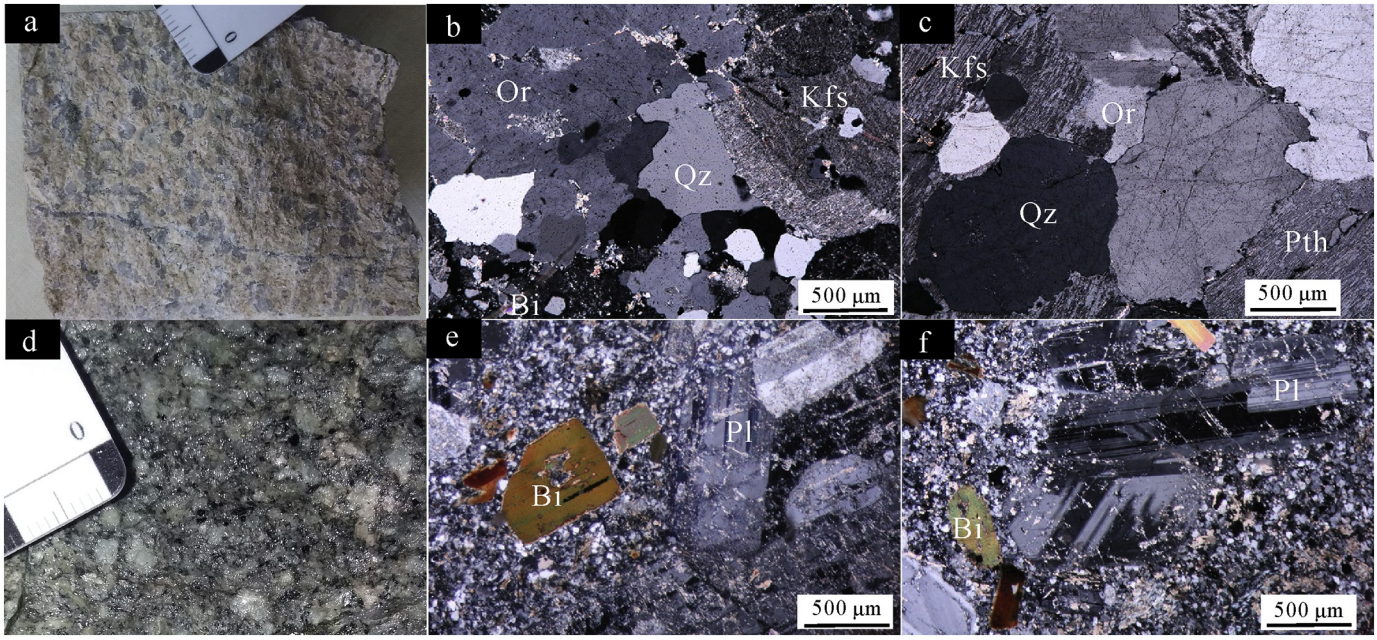

Fig. 3. (a) Hand specimen photograph and (b, c) photomicrographs of syenogranite; (d) hand specimen photograph and (e, f) photomicrographs of quartz diorite porphyry. Abbreviations: Pth = perthite; Pl = plagioclase; Or = orthoclase; Qz = quartz; Bt = biotite.

zircon U—Pb dating. Zircons were handpicked under a binocular microscope at Guangzhou Tuoyan Analytical Technology, Guangzhou, China. About 200 zircons for each sample were mounted in epoxy resin disks and polished for cathodoluminescence (CL) imaging with a scanning electron microscope (JSM–IT100) connected to a GATAN MiniCL system. Zircon U—Pb dating was undertaken at Wuhan Sample Solution Analytical Technology (WSSATCL), Wuhan, China, using a GeolasPro laser ablation system coupled to an Agilent 7700e inductively coupled plasma mass spectrometer (ICP–MS), with an ablation frequency of 5 Hz and spot diameter of 32 μm. Zircon 91,500 was used as an external standard for U—Pb age determinations and US National Institute of Standards and Technology (NIST) glass 610 was used for trace element calibrations. U—Pb and trace element analyses were processed with ICPMSDataCal software, following the method of Liu et al. (2010). Weighted-mean $^{206}Pb/^{238}U$ ages and concordia diagrams were produced using Isoplot/Ex Ver. 3 software (Ludwig, 2003). Zircon U—Pb isotopic data for the syenogranites and quartz diorite porphyries are given in Supplementary Table 1.

3.2. Whole-rock geochemical compositions

Nine samples of each rock type were collected for whole-rock geochemical analysis at WSSATCL. Major elements were analyzed by X-ray fluorescence (XRF) spectrometry on fused glass disks. Trace element compositions were determined by ICP–MS following the method of Gao et al. (2002). The analytical uncertainty for trace elements was better than ±10%, and for major elements better than ±1%. These analytical results are presented in Supplementary Table 2.

3.3. In situ zircon Hf isotopic analyses

Samples used for zircon U—Pb dating were also used for in situ Hf isotopic analysis at WSSATCL with a Neptune multi-collector ICP–MS equipped with a 193 nm laser, following the method of Hu et al. (2012). The laser ablation spot diameter was 50 μm, and a single spot ablation mode was used for all zircon analyses. Zircon 91,500 was again used for external standardization, yielding a weighted-mean $^{176}Hf/^{177}Hf$ ratio of 0.2823079 ± 0.0000049 (2σ; $n = 10$). Zircon Lu—Hf isotopic data for the Late Carboniferous syenogranites and Early Cretaceous quartz diorite porphyries are presented in Supplementary Table 3.

4. Results

4.1. LA–ICP–MS zircon U—Pb geochronology

Zircons in the syenogranites and quartz diorite porphyries are colorless to pale green and display significant oscillatory zoning typical of magmatic zircons (Fig. 4), with high Th/U ratios of 0.36–1.34 and 0.62–1.26, respectively, also indicating an igneous origin (Koschek, 1993).

Syenogranite samples BQH-9 and BQH-11 yielded weighted-mean $^{206}Pb/^{238}U$ ages of 319 ± 2 Ma ($n = 11$; MSWD = 0.32) and 319 ± 2 Ma ($n = 19$; MSWD = 0.61), respectively (Fig. 4a–d), with the age of 319 ± 2 Ma reflecting the crystallization age of the syenogranite.

Quartz diorite porphyry samples BQH-1 and BQH-5 yielded weighted-mean $^{206}Pb/^{238}U$ ages of 120 ± 1 Ma (MSWD = 0.40) and 120 ± 1 Ma (MSWD = 0.74), respectively (Fig. 4e–h), with the 120 ± 1 Ma age indicating that the quartz diorite porphyry was intruded during the Early Cretaceous.

4.2. Whole-rock geochemistry

Whole-rock geochemical data for the nine syenogranites and quartz diorite porphyries are plotted in Figs. 5a–b and 6a–d. Geochemical data for late Paleozoic A-type granites from the Songnen and Xing'an blocks reported by Guo et al. (2011), Shi et al. (2004), Wu et al. (2002), Zhang et al. (2013) and Zhao et al. (2013), and Early Cretaceous adakitic rocks from eastern NE China reported by Zhao et al. (2012) and Wang et al. (2019) are included in Figs. 5 and 6 for comparison.

4.2.1. Syenogranite

The Late Carboniferous syenogranites have high SiO_2 contents of 76.07–77.23 wt%, low $^{T}Fe_2O_3$ (0.56–1.19 wt%), CaO (0.08–0.25 wt%),

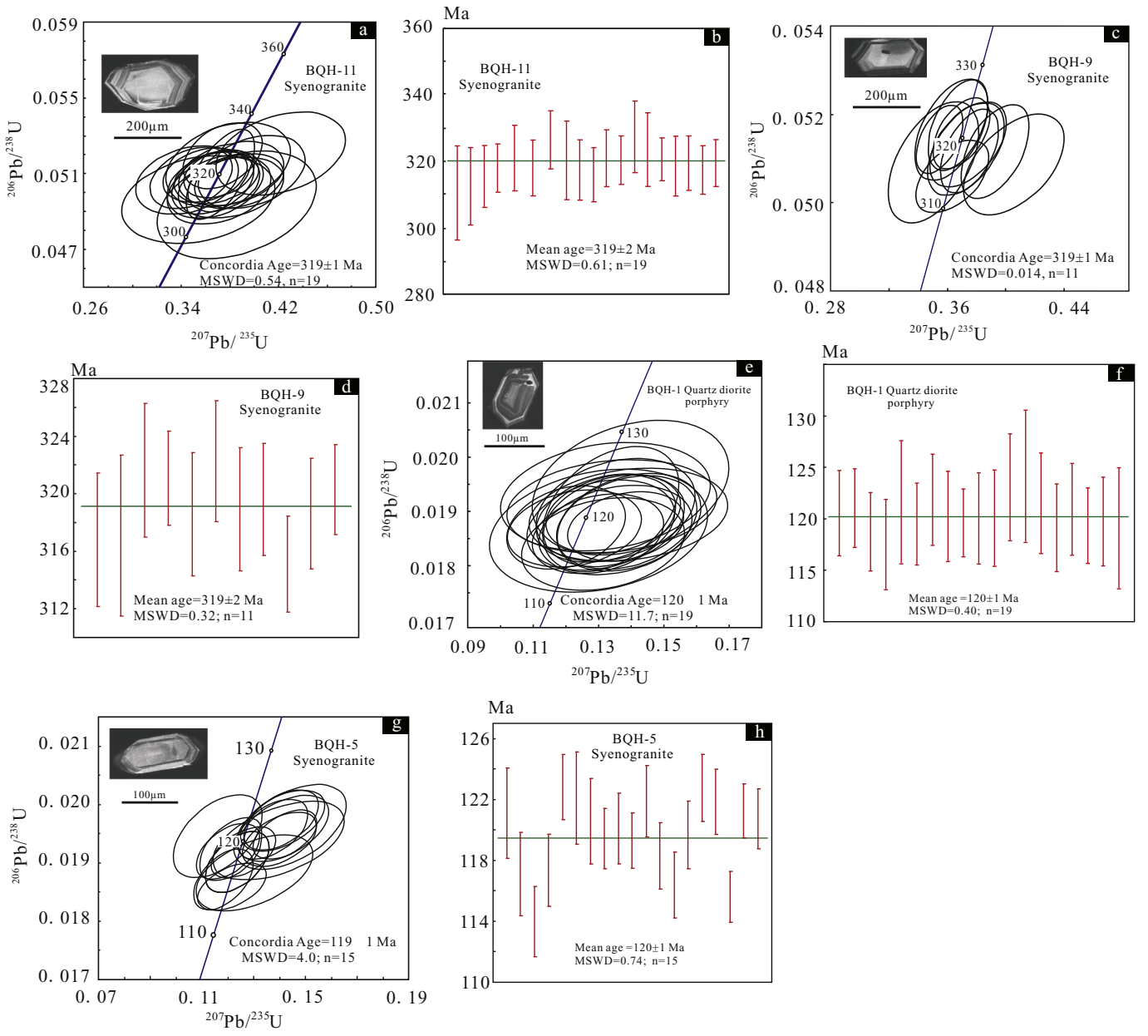

Fig. 4. Cathodoluminescence images, concordia diagrams, and weighted-mean zircon U—Pb ages of the (a–d) syenogranite and (e–h) quartz diorite porphyry of the northeastern Songnen Block.

and MgO (0.06–0.20 wt%) contents, and low $Mg^{\#}$ values of 14.5–36.7. They have high K_2O contents of 4.15–4.79 wt%, total alkali ($K_2O + Na_2O$) contents of 7.82–8.82 wt%, and K_2O/Na_2O ratios of 0.96–1.29 (average = 1.14) characteristic of K-rich granites (Barbarin, 1999), which plot in the high-K calc-alkaline field in a K_2O–SiO_2 diagram (Fig. 5a; Peccerillo and Taylor, 1976). They have Al_2O_3 contents of 11.75–12.87 wt% with A/CNK ($Al_2O_3/[CaO + Na_2O + K_2O]$) ratios of 1.00–1.15, typical of weakly peraluminous granite (Fig. 5b).

The chondrite-normalized rare earth element (REE) patterns (Fig. 6a) of the syenogranites exhibit light REE (LREE) and heavy REE (HREE) fractionation ($[La/Yb]_N$ = 4.69–7.06) and obvious negative Eu anomalies (Eu/Eu^* = 0.15–0.28). Primitive-mantle-normalized trace element patterns (Fig. 6b) exhibit depletion in Nb, Ta, P, and Ti, and enrichment in Rb, Th, U, K, and Ba.

4.2.2. Quartz diorite porphyry

The Early Cretaceous quartz diorite porphyry samples from the northeastern Songnen Block display little variation in SiO_2 contents (60.67–62.56 wt%), with high Na_2O (4.21–5.61 wt%), CaO (1.84–3.94 wt%), Al_2O_3 (16.30–16.71 wt%), and MgO (1.89–2.99 wt%) contents, and $Mg^{\#}$ values of 55–65. They plot in the calc-alkaline field in a K_2O–SiO_2 diagram (Fig. 5), with geochemical characteristics similar to those of Cretaceous adakitic rocks of eastern NE China (Fig. 5a–b). A/CNK ratios of 0.95–1.18 indicate a transition from being metaluminous to weakly peraluminous in the A/NK–A/CNK diagram (Fig. 5).

Chondrite-normalized REE and primitive-mantle-normalized trace element patterns (Fig. 6c–d) exhibit enrichment in LREE, depletion in HREE ($[La/Yb]_N$ = 14.8–22.7), negligible Eu anomalies (Eu/Eu^* = 0.82–1.18; Supplementary Table 2), depletion in Nb, Ta, Ti, and P, and

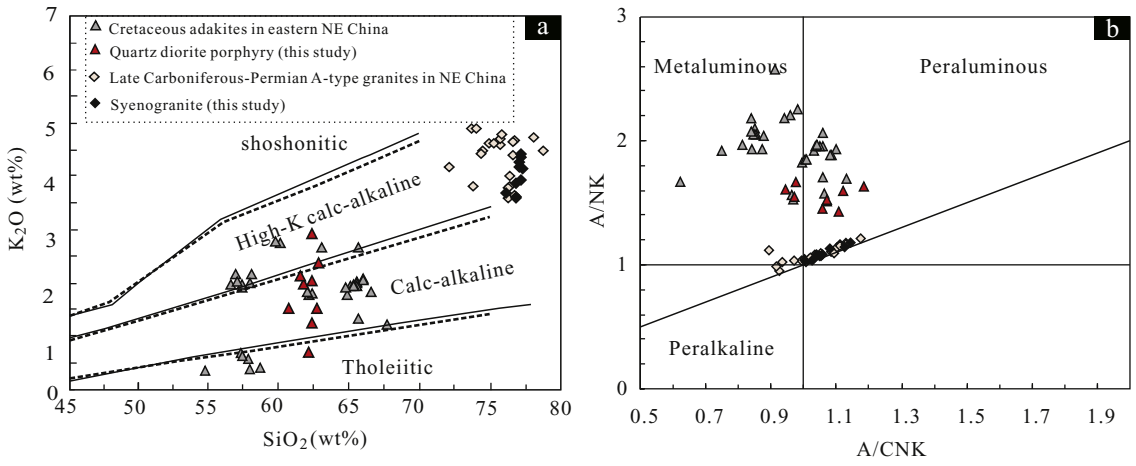

Fig. 5. (a) SiO_2–K_2O (Peccerillo and Taylor, 1976) and (b) (A/NK)–(A/CNK) diagrams (after Maniar and Piccoli, 1989) for the Late Carboniferous syenogranites and Early Cretaceous quartz diorite porphyries of the northeastern Songnen Block. Data for Cretaceous adakites of eastern NE China are from Zhao et al. (2013) and Wang et al. (2019); data for Late Carboniferous–Permian A-type granites of NE China are from Wu et al. (2002), Shi et al. (2004), Guo et al. (2011), Zhang et al. (2013), and Zhao et al. (2013).

enrichment in Rb, K, and Ba. Significantly, the Early Cretaceous quartz diorite porphyries have high Sr (589–1131 ppm) and low Yb (0.98–1.34 ppm) and Y (11.1–14.4 ppm) contents, typical of adakites (Sr > 400 ppm, Yb < 1.9 ppm, and Y < 18 ppm; Defant and Drummond, 1990; Fig. 7).

4.3. Zircon Hf isotopes

Zircon initial $^{176}Hf/^{177}Hf$ ratios for the syenogranites and quartz diorite porphyries are 0.282825–0.282923 and 0.282883–0.282918, with $\varepsilon_{Hf}(t)$ values of 8.4–12.1 and 6.5–7.7, respectively, and plot between chondrite and depleted mantle evolution lines in $\varepsilon_{Hf}(t)$–age diagrams (Fig. 8). The samples yielded two-stage model ages of 795–561 and 764–685 Ma, respectively (Supplementary Table 3).

5. Discussion

5.1. Petrogenesis

5.1.1. Late Carboniferous syenogranites from juvenile lower crust

Compared to typical I- and S-type granites described by Whalen et al. (1987) and King et al. (1997), the Late Carboniferous syenogranites of the northeastern Songnen Block have remarkably high HREE contents, significantly negative Eu anomalies, and low Sr

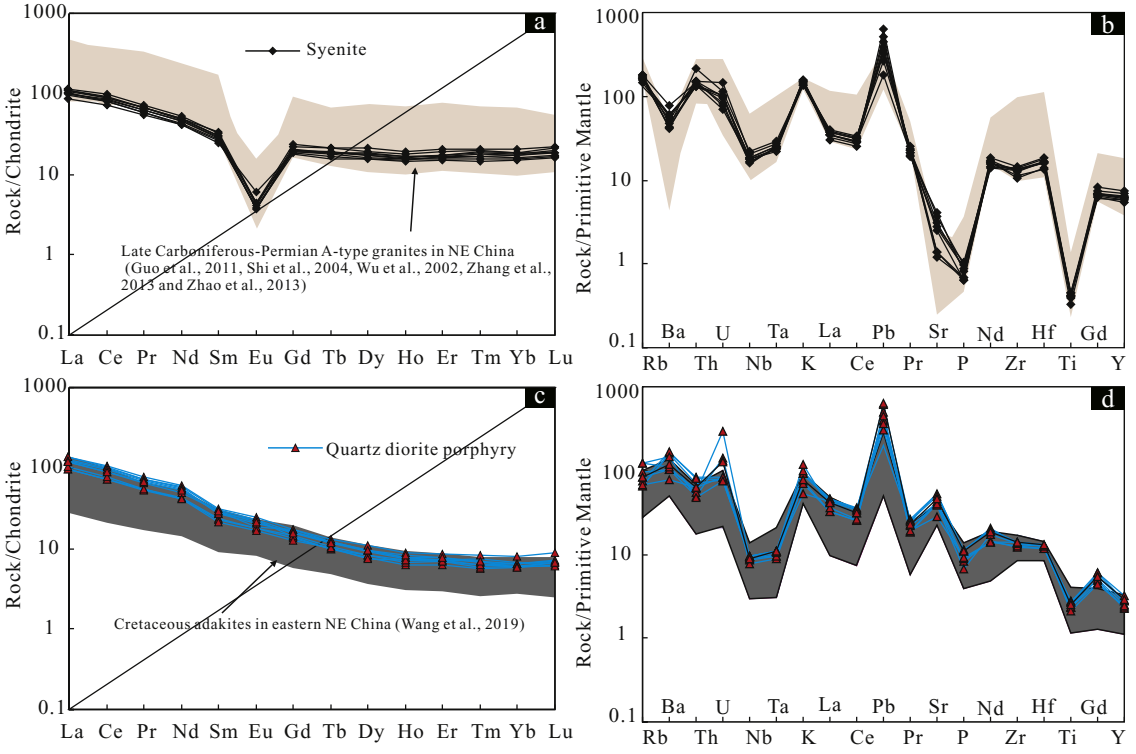

Fig. 6. (a) Chondrite-normalized REE patterns and (b) primitive-mantle-normalized spider diagrams for the Late Carboniferous syenogranites and Early Cretaceous quartz diorite porphyries of the northeastern Songnen Block. Chondrite and primitive mantle values are from Sun and McDonough (1989).

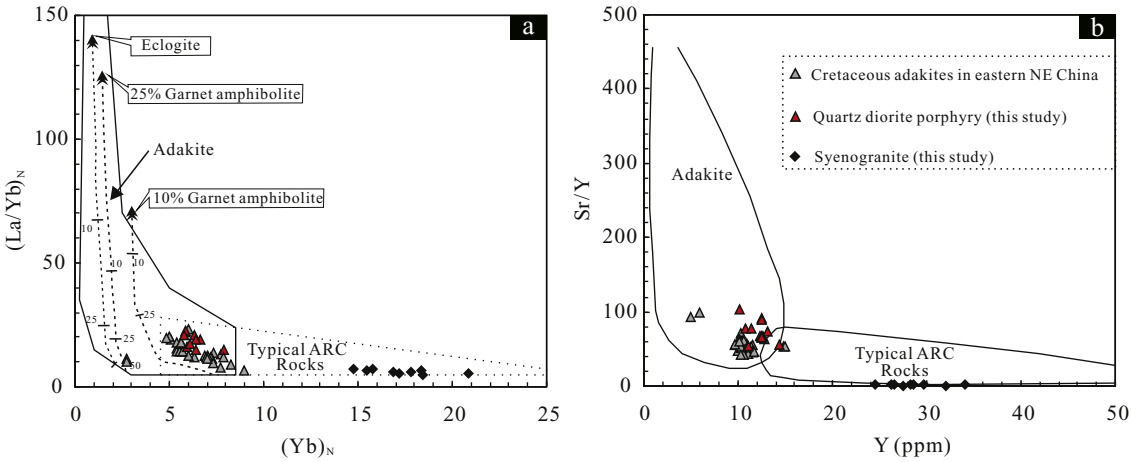

Fig. 7. (a) $(La/Yb)_N$–$(Yb)_N$ (after Drummond et al., 1996; N = normalized to chondrite; Sun and McDonough, 1989) and (b) (Sr/Y)–Y diagrams (after Defant and Drummond, 1990) for Late Carboniferous syenogranites and Early Cretaceous quartz diorite porphyries of the northeastern Songnen Block. Data for the Cretaceous adakites of eastern NE China are from Zhao et al. (2013) and Wang et al. (2019).

contents, with such characteristics being similar to those of A-type granites (Bonin, 2007; Eby, 1992; Whalen et al., 1987). Furthermore, in the commonly used A-type granite discrimination diagrams (Fig. 9a–d; Whalen et al., 1987; Frost et al., 2001; Wu et al., 2017), all syenogranite samples display $^{T}FeO/(^{T}FeO + MgO)$, $(K_2O + Na_2O)/CaO$, $^{T}FeO/MgO$, and Ga/Al ratios similar to those of late Paleozoic A-type granites of NE China (Guo et al., 2011; Ma et al., 2019; Shi et al., 2004; Wu et al., 2002; Zhang et al., 2013; Zhao et al., 2013).

Their high SiO_2 and low $^{T}Fe_2O_3$, MgO, Cr, and Ni contents (Supplementary Table 2), and the absence of coeval mafic igneous rocks indicate that the syenogranites were unlikely to have been generated through fractionation of upper mantle-derived magma as suggested by Bonin (2007). Small variations in whole-rock geochemistry (Supplementary Table 2) and a lack of inherited zircons also preclude an origin through magma mixing between mantle and crustal melts as proposed by Kemp et al. (2005). Rather, the syenogranites display geochemical characteristics similar to that of melt derived experimentally from the partial melting of crustal rocks (Patiño Douce, 1996). Their positive $\varepsilon_{Hf}(t)$ values (8.4–12.1; Supplementary Table 3) and two-stage model ages (795–561 Ma; Supplementary Table 3) imply a juvenile lower crustal source that was accreted during the Neoproterozoic.

Previous studies have shown that Late Carboniferous–early Permian A-type granites of NE China and adjacent areas were formed through fractional crystallization of magma (Tong et al., 2015; Zhang et al., 2015), as appears to be the case for the studied syenogranites. Their negative Eu anomalies and depletions in Sr, P, and Ti may have resulted from fractional crystallization during magma evolution. Negative Eu anomalies and Sr depletion are indicative of plagioclase fractionation; Ti depletion is usually related to fractionation of titanite; P depletion is due to fractionation of apatite. Furthermore, the high HREE contents and low $(La/Yb)_N$ ratios (4.69–7.06) indicate a garnet-free source, consistent with low Sr/Y ratios (0.90–2.89), and implying that the melts were generated at low pressures (Kay and Mpodozis, 2002).

5.1.2. Early Cretaceous quartz diorite porphyries from ocean slab melting

The Early Cretaceous quartz diorite porphyries from the northeastern Songnen Block have whole-rock geochemical characteristics similar to those of adakites, such as high Sr contents (589–1131 ppm), low Y and Yb contents (10–1404 and 0.98–1.34 ppm, respectively), and high Sr/Y ratios (Fig. 7a–b; Defant and Drummond, 1990). Their insignificant variations in SiO_2, Al_2O_3, and $^{T}Fe_2O_3$, and zircon $\varepsilon_{Hf}(t)$ values (6.5–7.1) preclude a derivation from the mixing of crustal and mantle melts

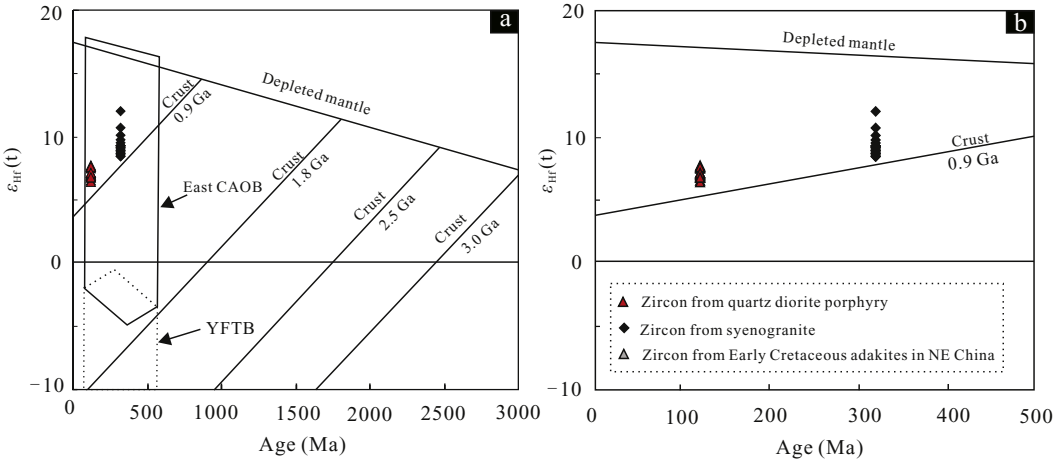

Fig. 8. $\varepsilon_{Hf}(t)$–age diagrams for zircons from the syenogranite and quartz diorite porphyry samples of the northeastern Songnen Block. YFTB = Yanshan Fold-and-Thrust Belt (Yang et al., 2006).

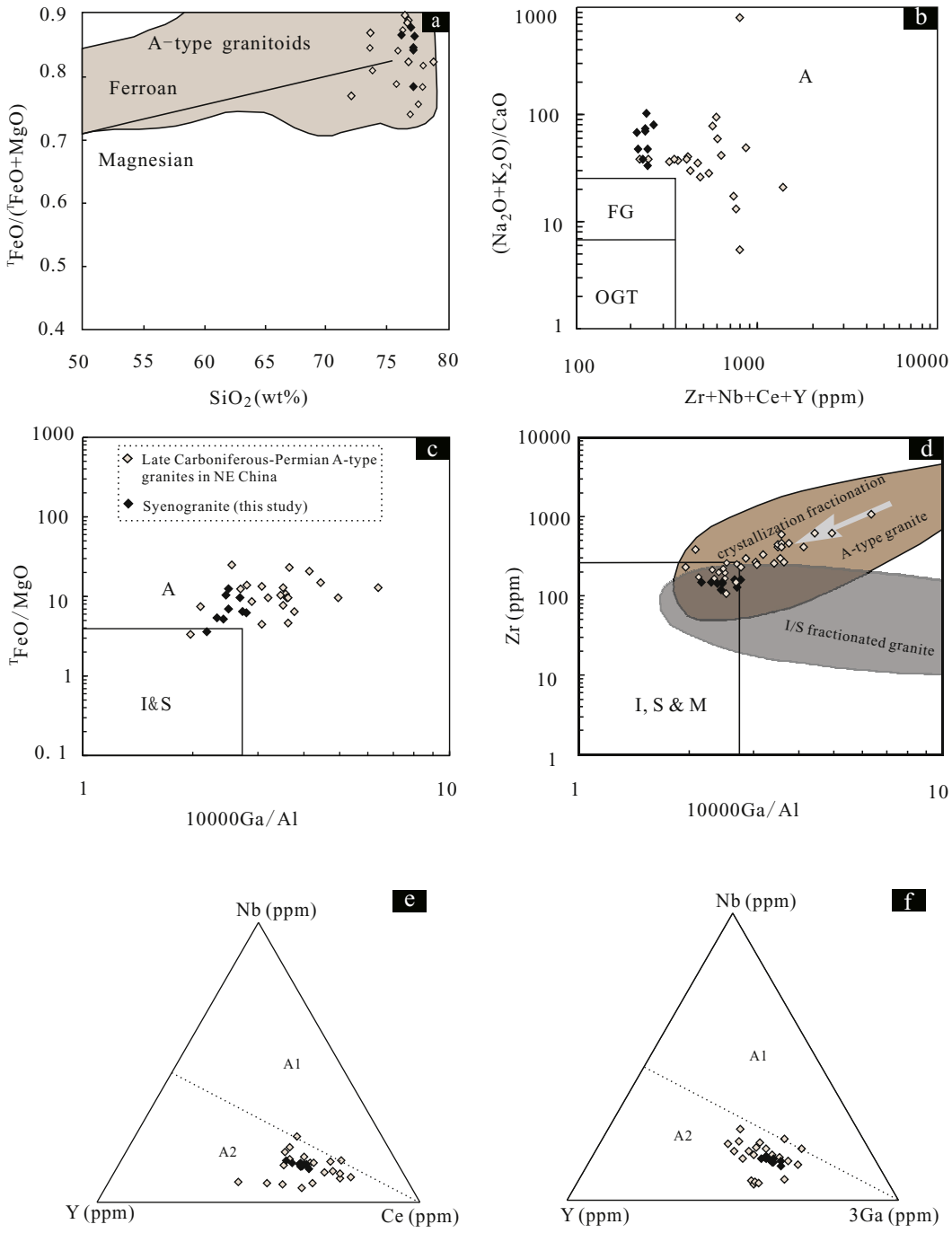

Fig. 9. (a, b) Discrimination diagrams for A-type granites (after Whalen et al., 1987; Frost et al., 2001) and (c, d) A1/A2 discrimination of A-type granites of the northeastern Songnen Block (after Eby, 1992). Data for Late Carboniferous–Permian A-type granites of NE China are from Wu et al. (2002), Shi et al. (2004), Guo et al. (2011), Zhang et al. (2013), and Zhao et al. (2013).

(e.g., Jiang et al., 2006; Wang et al., 2019). Experimental studies have shown that melts of metamorphosed basement associated with thickened lower crust generally have $Mg^{\#}$ values of <43 (Fig. 10; Rapp and Watson, 1995). Here, the quartz diorite porphyries have $Mg^{\#}$ values of 55–66 and higher Ni and Cr contents than adakites derived from thickened lower crust (Fig. 10). Moreover, they have low K_2O/Na_2O ratios (0.28–0.74; average = 0.55) and high CaO contents (1.84–3.94 wt%; average = 2.77 wt%), similar to those of oceanic slab-derived adakites described by Yogodzinski et al. (1995) and Stern and Kilian (1996). Significantly, Cu—Mo mineralization occurs in areas of quartz diorite porphyry stocks and adjacent syenogranite plutons. Previous studies have shown that porphyry Cu deposits in active convergent margin settings generally have strong affinities with oceanic slab-derived adakites (Sun et al., 2011). This was further supported by Zhao et al. (2012) who studied the petrogenesis of Early Cretaceous ore-forming adakitic diorite porphyries associated with the Jinchang porphyry Au—Cu deposit and proposed an oceanic slab-melt source for these adakites.

The quartz diorite porphyries have low Nb/Zr and Nb/Ti and high Ba/Ce and Ba/Zr ratios, which plot between enriched mantle and subduction components (Fig. 11a–b), further suggesting they were generated by partial melting of oceanic crust, with a degree of interaction with mantle-derived melts. The lack of inherited zircons and positive zircon $\varepsilon_{Hf}(t)$ values (6.5–7.1) indicate limited contamination by continental

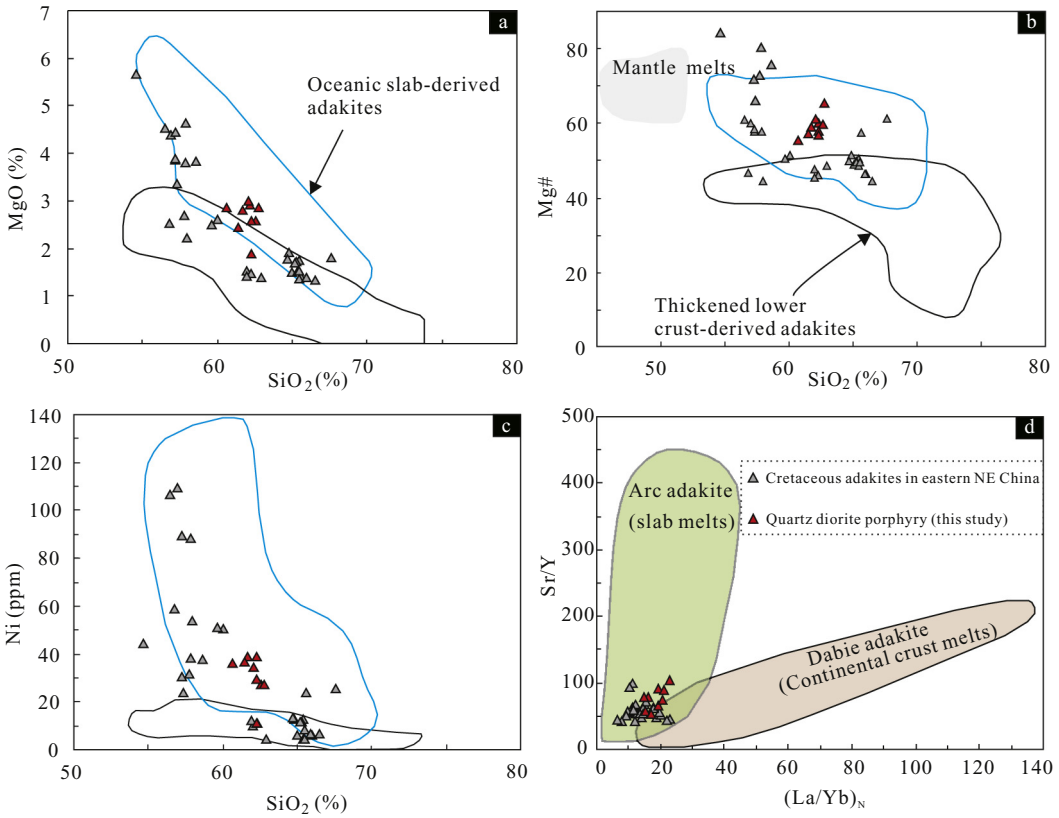

Fig. 10. Diagrams illustrating the differences between adakites derived from an oceanic slab and thickened lower crust. (a) MgO–SiO_2 diagram (after Wang et al., 2006). (b) $Mg^{\#}$–SiO_2 diagram (after Long et al., 2015). (c) Ni–SiO_2 diagram (after Wang et al., 2006). (d) (Sr/Y)–$(La/Yb)_N$ diagram (after Sun et al., 2012, 2018). Data for Cretaceous adakites of eastern NE China are from Zhao et al. (2012) and Wang et al. (2019).

crust. Their trace element and REE compositions, with enrichment in Sr, depletion in Y and HREE, and concave middle REE (MREE) patterns, suggest both amphibole and garnet were present in the source (e.g., Mao et al., 2018; Oh et al., 2016). The low Nb/Ta (14.38–16.79) and Zr/Sm (31.03–46.74) ratios suggest the melting of amphibolite rather than eclogite (Martin et al., 2005), indicating that the magma was derived from a shallow oceanic slab.

5.2. Implications for geodynamic evolution

5.2.1. Final closure of the Paleo-Asian Ocean

At least four stages of A-type granites have been reported in NE China: Early Ordovician (Deng et al., 2018b; Wu et al., 2019); Late Carboniferous–Permian (Li et al., 2014; Ma et al., 2019; Zhang et al., 2013); Late Triassic–Early Jurassic (Wu et al., 2002); Cretaceous (Ji

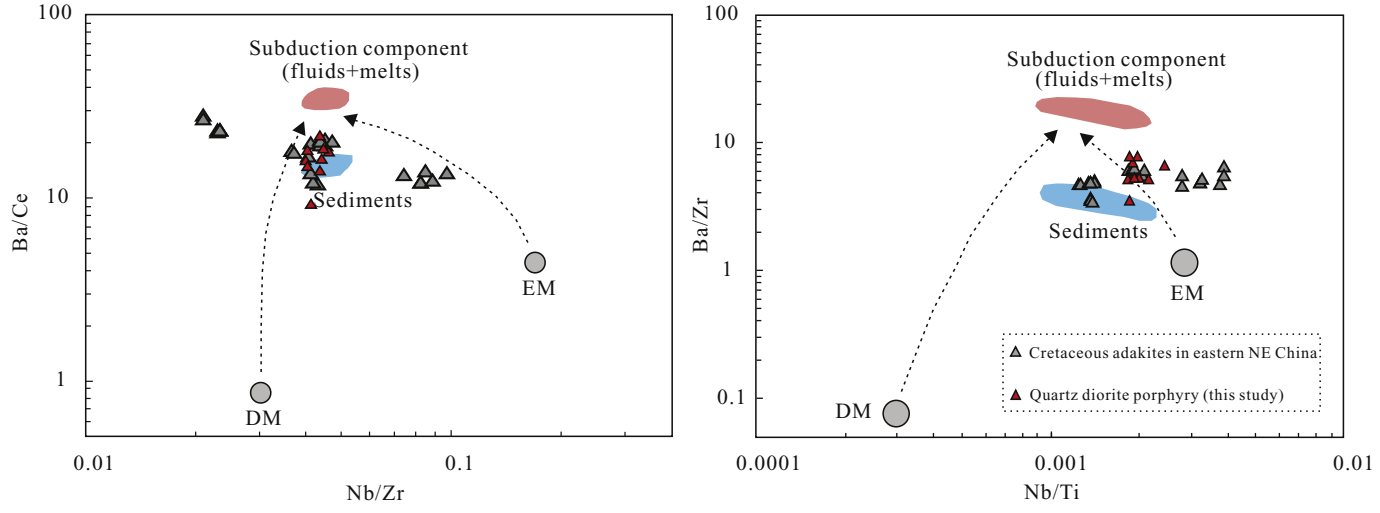

Fig. 11. (a) (Ba/Ce)–(Nb/Zr) and (b) (Ba/Zr)–(Nb/Ti) diagrams for quartz diorite porphyry (after Ferrari et al., 2001). Data for Cretaceous adakites of eastern NE China are from Wang et al. (2019).

et al., 2019; Wang et al., 2019; Wu et al., 2002). Unlike the irregular spatial distribution of A-type granites of other stages, the Late Carboniferous–Permian A-type granites are mainly distributed along the Hegenshan–Heihe Suture Zone (Ma et al., 2019; Tong et al., 2015; Zhang et al., 2015), which is considered to have formed after final closure of the Paleo-Asian Ocean between the Xing'an and Songnen blocks (Li et al., 2014; Ma et al., 2019; Tong et al., 2015; Wu et al., 2002; Zhang et al., 2015; Zhao et al., 2010). The petrogenesis of these particular granites may therefore elucidate key stages of the tectonic evolution of the Paleo-Asian Ocean.

Previous studies have indicated that A-type granites were generally produced in post-collisional or intraplate extensional settings (Eby, 1992; Wu et al., 2002). Eby (1992) subdivided A-type granites into mantle-derived A_1 and crust-derived A_2 subgroups according to their different origins. The former was generally emplaced in an intraplate tectonic setting with Y/Nb ratios of <1.2, while the latter was likely produced in post-collision or back-arc tectonic environments with higher Y/Nb ratios (Eby, 1992). The Late Carboniferous syenogranites have high Y/Nb ratios (2.07–2.40) and plot in the A_2 subgroup field in the Ce–Nb–Y diagram (Fig. 9e, f; Eby, 1992), similar to Late Carboniferous–Permian A-type granites distributed along the Hegenshan–Heihe Suture Zone (Ma et al., 2019; Wu et al., 2002; Zhang et al., 2013), indicating that these A-type granites formed in similar tectonic environments. Zhao et al. (2010) suggested that the stratigraphic transformation from early Carboniferous marine sediment to Late Carboniferous continental sediment was likely related to the collision and merging of the Songnen and Erguna–Xing'an blocks, which is supported by geochemical and isotopic data for Late Carboniferous–Permian A-type granites formed in a post-collision extensional setting (Ma et al., 2019; Wu et al., 2002). This is consistent with our syenogranite samples plotting in the post-collisional rather than volcanic arc field in the Rb–(Y + Nb) diagram (Fig. 12; Pearce, 1996). Liu et al. (2017) proposed that ridge subduction during the Late Devonian may have caused large-scale magma underplating in the Late Carboniferous–Permian in east Junggar, NW China, but Paleozoic ridge subduction has not yet been confirmed in the study area. Overall, a post-collision setting appears to provide a reasonable explanation of the distribution of Late Carboniferous–Permian A-type granites along the Hegenshan–Heihe Suture Zone. This is also supported by previous studies that suggested that late Paleozoic A-type granites in NE China and Central Inner Mongolia were formed in a post-collision extensional setting (Ma et al., 2019; Tong et al., 2015; Zhang et al., 2015). Considering that the Early Cretaceous igneous rocks in the eastern CAOB have geochemical characteristics similar to those of subduction-related I-type granites (Gou et al., 2013; Zhou and Wilde, 2013), we infer that the tectonic shift of the Paleo-Asian Ocean between the Songnen and Xing'an blocks, from plate subduction to closure, likely occurred during the late early–early Late Carboniferous. Based on this, we suggest that final closure of the Paleo-Asian Ocean between the Songnen and Xing'an blocks occurred prior to the Late Carboniferous.

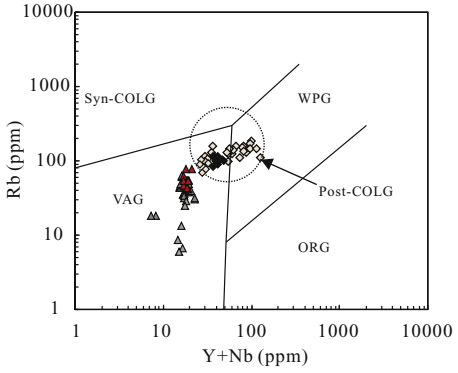

Fig. 12. Rb–(Y + Nb) diagrams (Pearce, 1996) for syenogranite and quartz diorite porphyry samples of the northeastern Songnen Block. Abbreviations: ORG = ocean ridge granite; WPG = within-plate granite; VAG = volcanic arc granite; Syn COLG = *syn*-collisional granite; Post-COLG = post-collisional granite. The symbols and data sources are as in Fig. 5.

5.2.2. Evolution of the residual Paleo-Pacific flat slab and its implications

Previous studies have indicated that flat slab subduction of the Paleo-Pacific Plate beneath eastern Eurasia occurred during the Late Jurassic (Maruyama et al., 1997; Zhang et al., 2011; Fig. 13a), as supported by the Middle Jurassic–early Early Cretaceous magmatic gap in eastern NE China (Kiminami and Imaoka, 2013; Fig. 13a). A slab rollback model for the Paleo-Pacific Ocean during the late Early–Late Cretaceous was suggested as the causative mechanism for the temporospatial migration of late Mesozoic extension-related magmatism in NE China (Ji et al., 2019; Wang et al., 2019). However, few studies have considered the key subduction stage of the Paleo-Pacific Plate during the switch from flat to steep subduction.

Geochemical characteristics of our quartz diorite porphyry samples indicate that oceanic slab melts were involved, supported by an earlier suggestion that oceanic slab-derived melts had an important role in the generation of adakitic andesites (114–110 Ma) in eastern NE China (Wang et al., 2019). Considering the low Nb/Ta and Zr/Sm ratios of the quartz diorite porphyry and low garnet content of the magma source (Fig. 7a), we conclude that partial melting of the oceanic slab occurred at a relatively shallow depth (e.g., Li et al., 2016). Compared with coeval mantle-derived andesite in the adjacent area (MgO, Cr, and Ni contents of 2.22–4.53 wt%, 102–299 ppm, and 51–109 ppm, respectively; Wang et al., 2019), the lower MgO (1.89–2.92 wt%), Cr (13.2–49.8 ppm), and Ni (11.2–39.0 ppm) contents of the Early Cretaceous quartz diorite porphyries from the northeastern Songnen Block indicate limited interaction between slab-derived melts and mantle peridotites (e.g., Stern and Kilian, 1996), implying the existence of a thin mantle wedge as in the model proposed by Gutscher et al. (2000) (Fig. 13b).

It has been suggested that acceleration of subduction of the Paleo-Pacific Plate triggered steep subduction (Wang et al., 2019). The drag force from the steeper slab led to the deformation and downwarping of the Paleo-Pacific flat slab, triggering dehydration, eclogitization, and partial melting of the slab (Fig. 13c). A sinking slab commonly generates upwelling of asthenospheric mantle to compensate for the loss of mantle volume (Hamilton, 2007). Together with fluids derived from the flat slab, this would have led to large-scale partial melting of the metasomatized mantle and lower continental crust (Fig. 13c), forming the ca. 120–105 Ma volcanic rocks of eastern NE China (Wang et al., 2019). With completion of the trench-ward eclogitization of the residual Paleo-Pacific flat slab, volcanism in the interior continent would have gradually ceased (Fig. 13d). Considering that the temporospatial migration of volcanism in NE China is consistent with the eastward eclogitization of the residual Paleo-Pacific flat slab, we propose that the dehydration and eclogitization processes of the residual flat slab, together with rollback of Paleo-Pacific Plate, played an important role in controlling the formation and temporospatial migration of Cretaceous igneous rocks in NE China.

6. Conclusions

This study led to the following key conclusions.

(1) Late Carboniferous A-type granites and Early Cretaceous adakites occur in the northeastern Songnen Block.
(2) The A-type granites were derived by partial melting of juvenile basaltic lower crust, while the adakites were produced by partial melting of an oceanic slab with a degree of contamination by the mantle wedge.

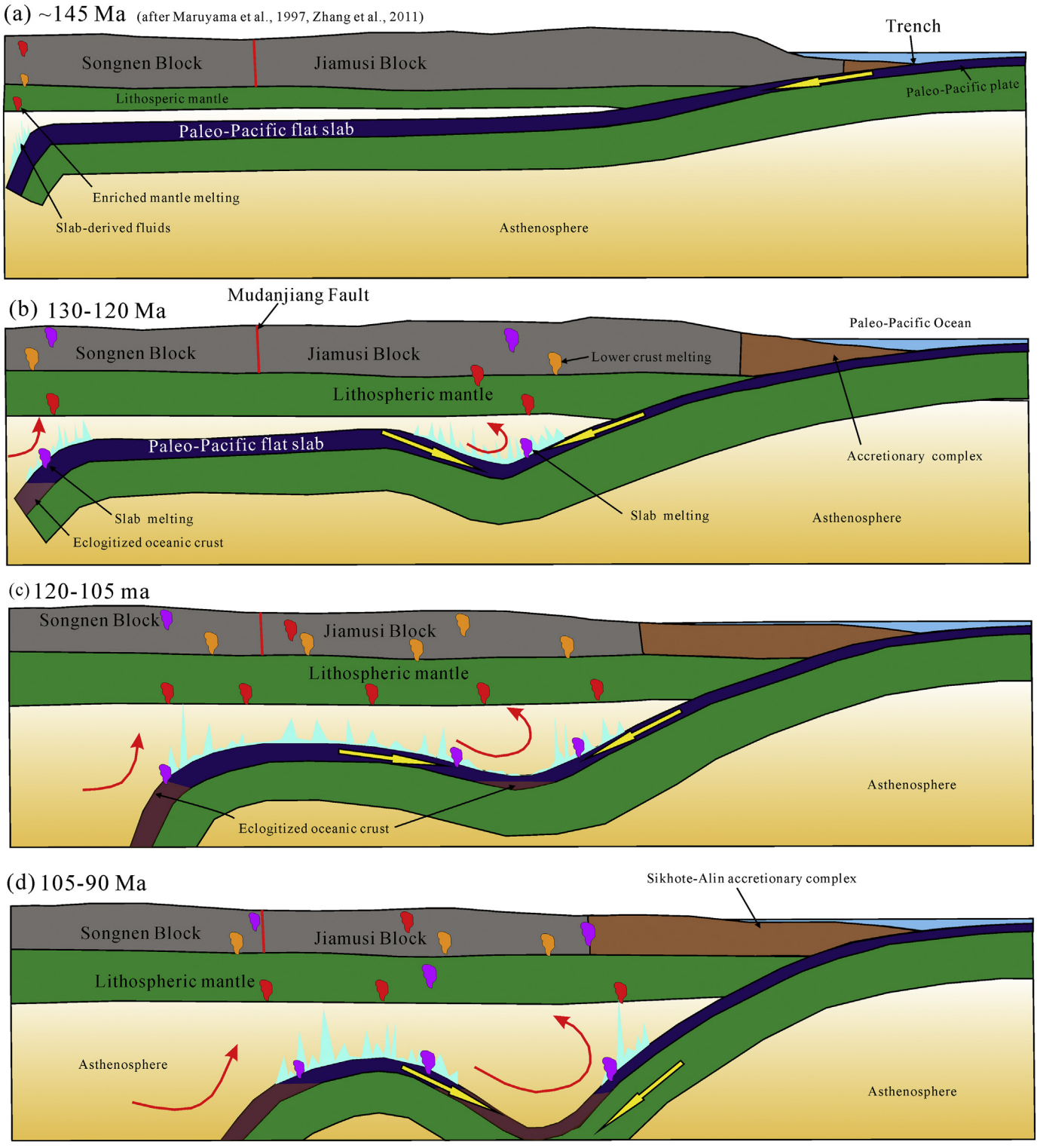

Fig. 13. Diagrammatic depictions of the evolution of westward subduction of the Paleo-Pacific Plate beneath NE China during the Early–Late Cretaceous.

(3) The petrogenesis of the late Paleozoic A-type granites along the Hegenshan–Heihe Suture Zone indicates that final closure of the Paleo-Asian Ocean between the Songnen and Xing'an blocks occurred before the Late Carboniferous.
(4) The occurrence of Early Cretaceous adakites in eastern NE China indicates that the residual Paleo-Pacific oceanic flat slab has an important role in controlling the generation of Cretaceous igneous rocks in the interior of the NE China continent.

Supplementary data to this article can be found online at https://doi.org/10.1016/j.lithos.2020.105575.

Declaration of Competing Interest

The authors declare that they have no known competing financial interests or personal relationships that could have appeared to influence the work reported in this paper.

Acknowledgments

We are very grateful to Professor Qing Xiong and the anonymous reviewer for their constructive comments and suggestions on the manuscript. Editor-in-chief Xian-Hua Li is greatly acknowledged for his helpful comments. This work was supported by the Heilongjiang Research Project of Land and Resources (201701 and 2017030).

References

Barbarin, B., 1999. A review of the relationships between granitoid types, their origins and their geodynamic environments. Lithos 46, 605–626.
Bonin, B., 2007. A-type granites and related rocks: evolution of a concept, problems and prospects. Lithos 97, 1–29.
Chen, Y.J., Zhang, C., Wang, P., Pirajno, F., Li, N., 2017a. The Mo deposits of Northeast China: a powerful indicator of tectonic settings and associated evolution trends. Ore Geol. Rev. 81, 602–640.
Chen, X., Liu, J.J., Zhang, D.H., Zhang, Q.B., Yang, S.S., Li, Y.C., Cao, Q., 2017b. Re-Os dating of molybdenites and S-Pb isotopic characteristics of the Cuihongshan iron polymetallic deposit, Heilongjiang Province. Acta Petrol. Sin. 33, 529–544.
Defant, M.J., Drummond, M.S., 1990. Derivation of some modern arc magmas by melting of young subducted lithosphere. Nature 347, 662–665.
Deng, C.Z., Sun, G.Y., Sun, D.Y., Huang, H., Zhang, J.F., Gou, J., 2018a. Origin of C type adakite magmas in the NE Xing'an block, NE China and tectonic implication. Acta Geochimica 37, 281–294.
Deng, C.Z., Sun, D.Y., Sun, G.Y., Lv, C.L., Qin, Z., Ping, X.Q., Li, G.H., 2018b. Age and geochemistry of Early Ordovician A-type granites in the northeastern Songnen Block, NE China. Acta Geochimica 37, 805–819.
Deng, C.Z., Sun, D.Y., Han, J.S., Chen, H.Y., Li, G.H., Xiao, B., Li, R.C., Feng, Y.Z., Li, C.L., Lu, S., 2019. Late-stage southwards subduction of the Mongol-Okhotsk oceanic slab and implications for porphyry Cu-Mo mineralization: constraints from igneous rocks associated with the Fukeshan deposit, NE China. Lithos 326–327, 341–357.
Drummond, M.S., Defant, M.J., Kepezhinskas, P.K., 1996. Petrogenesis of slab-derived trondhjemite–tonalite–dacite/adakite magmas. Transactions of the Royal Society of Edinburgh-Earth Sciences 87, 205–215.
Eby, G.N., 1992. Chemical subdivision of the A-type granitoids: petrogenetic and tectonic implications. Geology 20, 641–644.
Ferrari, L., Petrone, C.M., Francalanci, L., 2001. Generation of oceanic-island basalt–type volcanism in the western Trans-Mexican volcanic belt by slab rollback, asthenosphere infiltration, and variable flux melting. Geology 29, 507–510.
Frost, B.R., Barnes, C.G., Collins, W.J., Arculus, R.J., Ellis, D.J., Frost, C.D., 2001. A geochemical classification for granitic rocks. J. Petrol. 42, 2033–2048.
Gao, S., Liu, X.M., Yuan, H.L., Hattendorf, B., Gunther, D., Chen, L., Hu, S.H., 2002. Determination of forty-two major and trace elements in USGS and NIST SRM glasses by laser ablation-inductively coupled plasma-mass spectrometry. Geostand. Newslett. J. Geostand. Geoanal. 26, 191–196.
Ge, W.C., Wu, F.Y., Zhou, C.Y., Rahman, A.A.A., 2005. Emplacement age of the Tahe granite and its constraints on the tectonic nature of the Ergun block in the northern part of the Da Hinggan Range. Chin. Sci. Bull. 50, 2097–2105.
Gou, J., Sun, D.Y., Ren, Y.S., Liu, Y.J., Zhang, S.Y., Fu, C.L., Wang, T.H., Wu, P.F., Liu, X.M., 2013. Petrogenesis and geodynamic setting of Neoproterozoic and Late Paleozoic magmatism in the Manzhouli–Erguna area of Inner Mongolia, China: geochronological, geochemical and Hf isotopic evidence. J. Asian Earth Sci. 67–68, 114–137.
Guo, K.C., Zhang, W.L., Yang, X.P., Wang, L., Shi, D.Y., Yu, H.T., Su, H., 2011. Origin of Early Permian A-type Granite in the Wudaogou Area, Heihe City. J. Jilin Univ. (Earth Sci. Ed.) 41, 1077–1083 (in Chinese with English abstract).
Gutscher, M.A., Maury, R., Eissen, J.P., Bourdon, E., 2000. Can slab melting be caused by flat subduction? Geology 28, 535–538.
Hamilton, W., 2007. Driving mechanism and 3-D circulation of plate tectonics. In: Sears, J.W., Harms, T.A., Evenchick, C.A. (Eds.), Whence the Mountains? Inquiries Into the Evolution of Orogenic Systems: A Volume in Honor of Raymond A. Price. 433. Geological Society of America, pp. 1–25 Special Paper.
HBGMR, 1997. Heilongjiang bureau of geology and mineral resources. Rock Stratigraphic Units. China university of Geoscience Press, Wuhan (in Chinese with English abstract).
Hu, Z.C., Liu, Y.S., Gao, S., Liu, W.G., Yang, L., Zhang, W., Tong, X.R., Lin, L., Zong, K.Q., Li, M., Chen, H.H., Zhou, L., 2012. Improved in situ Hf isotope ratio analysis of zircon using newly designed X skimmer cone and Jet sample cone in combination with the addition of nitrogen by laser ablation multiple collector ICP-MS. J. Anal. At. Spectrom. 27, 1391–1399.
Jahn, B.M., 2004. The Central Asian Orogenic Belt and growth of the continental crust in the Phanerozoic. Geol. Soc. Lond. Spec. Publ. 226, 73–100.
Ji, Z., Meng, Q.A., Wan, C.B., Ge, W.C., Yang, H., Zhang, Y.L., Dong, Y., Jin, X., 2019. Early Cretaceous adakitic lavas and A-type rhyolites in the Songliao Basin, NE, China: implications for the mechanism of lithospheric extension. Gondwana Res. 71, 28–48.
Jiang, Y.H., Jiang, S.Y., Ling, H.F., Dai, B.Z., 2006. Low-degree melting of a metasomatized lithospheric mantle for the origin of Cenozoic Yulong monzogranite-porphyry, East Tibet: geochemical and Sr–Nd–Pb–Hf isotopic constraints. Earth Planet. Sci. Lett. 241, 617–633.
Kay, S.M., Mpodozis, C., 2002. Central andean ore deposits linked to evolving shallow subduction systems and thickening crust. GSA Today 11, 4–11.
Kemp, A.I.S., Wormald, R.J., Whitehouse, M.J., Price, R.C., 2005. Hf isotopes in zircon reveal contrasting sources and crystallization histories for alkaline to peralkaline granites of Temora, southeastern Australia. Geology 33, 797–800.
Kiminami, K., Imaoka, T., 2013. Spatiotemporal variations of Jurassic–Cretaceous magmatism in eastern Asia (Tan-Lu Fault to SW Japan): evidence for flat-slab subduction and slab rollback. Terra Nova 25, 414–422.
King, P.L., White, A.J.R., Chappell, B.W., Allen, C.M., 1997. Characterization and origin of aluminous A-type granites from the Lachlan Fold Belt, southeastern Australia. J. Petrol. 38, 371–391.
Koschek, G., 1993. Origin and significance of the SEM cathodoluminescence from zircon. J. Microsc. 171, 223–232.
Li, C.L., Qu, H., Zhao, Z.H., Xu, G.Z., Wang, Z., Zhang, J.F., 2013. Zircon U-Pb ages, geochemical characteristics and tectonic implications of Early Carboniferous granites in Huolongmen area, Heilongjiang Province. Geol. China 40, 859–868 (in Chinese with English abstract).
Li, J.Y., Guo, F., Li, H.X., Zhao, L., 2014. Neodymium isotopic variations of Late Paleozoic to Mesozoic I- and A-type granitoids in NE China: Implications for tectonic evolution. Acta Petrol. Sin. 30, 1995–2008 (in Chinese with English abstract).
Li, S.M., Zhu, D.C., Wang, Q., Zhao, Z.D., Zhang, L.L., Liu, S.A., Chang, Q.S., Lu, Y.H., Dai, J.G., Zheng, Y.C., 2016. Slab-derived adakites and subslab asthenosphere-derived OIB-type rocks at 156 ± 2 Ma from the north of Gerze, Central Tibet: records of the Bangong-Nujiang oceanic ridge subduction during the Late Jurassic. Lithos 262, 456–469.
Liu, J.F., Chi, X.G., Dong, C.Y., Zhao, Z., Li, G.R., Zhao, Y.D., 2008. Discovery of Early Paleozoic granites in the eastern Xiao Hinggan Mountains, northeastern China and their tectonic significance. Geol. Bull. China 27 (4), 534–544 (in Chinese with English abstract).
Liu, Y.S., Gao, S., Hu, Z.C., Gao, C.G., Zong, K.Q., Wang, D.B., 2010. Continental and oceanic crust recycling-induced melt-peridotite interactions in the Trans-North China Orogen: U-Pb dating, Hf isotopes and trace elements in zircons of mantle xenoliths. J. Petrol. 51, 537–571.
Liu, X.J., Xiao, W.J., Xu, J.F., Castillo, P.R., Shi, Y., 2017. Geochemical signature and rock associations of ocean ridge-subduction: evidence from the Karamaili Paleo-Asian ophiolite in east Junggar, NW China. Gondwana Res. 48, 34–49.
Long, X., Wilde, S.A., Wang, Q., Yuan, C., Wang, X.C., Li, J., Jiang, Z., Dan, W., 2015. Partial melting of thickened continental crust in Central Tibet: evidence from geochemistry and geochronology of Eocene adakitic rhyolites in the northern Qiangtang terrane. Earth Planet. Sci. Lett. 414, 30–44.
Ludwig, K.R., 2003. ISOPLOT 3.00: A Geochronological Toolkit for Microsoft Excel. Berkeley Geochronology Center, California, Berkeley, p. 39.
Ma, Y.F., Liu, Y.J., Wang, Y., Qian, C., Si, Q.L., Tang, Z., Qin, T., 2019. Geochronology, petrogenesis, and tectonic implications of Permian felsic rocks of the Central Great Xing'an Range, NE China. Int. J. Earth Sci. 108, 427–453.
Maniar, P.D., Piccoli, P.M., 1989. Tectonic discrimination of granitoids. Geol. Soc. Am. Bull. 101, 635–643.
Mao, Q.G., Yu, M.J., Xiao, W.J., Windley, B.F., Li, Y.C., Wei, X.F., Zhu, J.J., Lü, X.Q., 2018. Skarn-mineralized porphyry adakites in th Harlik arc Kalatage, E. Tianshan (NW China): slab melting in the Devonian-early Carboniferous in the southern Central Asian Orogenic Belt. J. Asian Earth Sci. 153, 365–378.
Martin, H., Smithies, R.H., Rapp, R., Moyen, J.F., Champion, D., 2005. An overview of adakite, tonalite–trondhjemite–granodiorite (TTG), and sanukitoid: relationships and some implications for crustal evolution. Lithos 79, 1–24.
Maruyama, S., Isozaki, Y., Kimura, G., Terabayashi, M., 1997. Paleogeographic maps of the Japanese Islands: plate tectonic synthesis from 750 Ma to the present. Island Arc 6, 121–142.
Miao, L.C., Fan, W.M., Zhang, F.Q., et al., 2003. Zircon SHRIMP geochronology of the Xinkailing-Keluo complex in the northwestern Lesser Xing'an Range, and its geological implications. Chin. Sci. Bull. 48 2315–232 (in Chinese with English abstract).
Oh, J.I., Choi, S.H., Yi, K., 2016. Origin of adakite-like plutons in southern Korea. Lithos 262, 620–635.
Ouyang, H.G., Mao, J.W., Santosh, M., Zhou, J., Zhou, Z.H., Wu, Y., Hou, L., 2013. Geodynamic setting of Mesozoic magmatism in NE China and surrounding regions: perspectives from spatio-temporal distribution patterns of ore deposits. J. Asian Earth Sci. 78, 222–236.
Patiño Douce, A.E., 1996. Effects of pressure and H2O content on the compositions of primary crustal melts. Transactions of the Royal Society of Edinburgh. Earth Sci. 87, 11–21.
Pearce, J.A., 1996. Sources and settings of granitic rocks. Episodes 19, 120–125.
Peccerillo, A., Taylor, S.R., 1976. Geochemistry of Eocene calc-alkaline volcanic rocks from the Kastamonu area, northern Turkey. Contrib. Mineral. Petrol. 58, 63–81.
Rapp, R.P., Watson, E.B., 1995. Dehydration melting of metabasalt at 8–32 kbar: implications for continental growth and crustal recycling. J. Petrol. 36, 891–931.
Sengör, A.M.C., Natal'in, B.A., Burtman, V.S., 1993. Evolution of the Altaid tectonic collage and Palaeozoic crustal growth in Eurasia. Nature 364, 299–307.
Sengör, A.M.C., Natal'in, B.A., Sunal, G., van der Voo, R., 2018. The tectonics of the Altaids: Crustal growth druting the construction of the continental lithosphere of Central Asia between ~750 Ma and ~130 Ma ago. Annu. Rev. Earth Planet. Sci. 46, 439–494.
Shi, G.H., Miao, L.C., Zhang, F.Q., Jian, P., Fan, W.M., Liu, D.Y., 2004. The age and its district tectonic implications on the Xilinhaote A-type granites, Inner Mongolia. Chin. Sci. Bull. 49, 384–389 (in Chinese).

Stern, C.R., Kilian, R., 1996. Role of the subducted slab, mantle wedge and continental crust in the generation of adakites from the Andean austral volcanic zone. Constrib. Mineral. Petr. 123, 263–281.
Sun, S.S., McDonough, W.F., 1989. Chemical and isotopic systematics of oceanic basalts: Implications for mantle composition and process. In: Sauders, A.D., Norry, M.J. (Eds.), Magmatism in the Ocean Basins. 42. Geological Society Special Publication, pp. 313–345.
Sun, W.D., Zhang, H., Ling, M.X., Ding, X., Chung, S.L., Zhou, J.B., Yang, X.Y., Fan, W.M., 2011. The genetic association of adakites and Cu-Au ore deposits. Int. Geol. Rev. 53, 691–703.
Sun, W.D., Ling, M.X., Chung, S.L., Ding, X., Yang, X.Y., Liang, H.Y., Fan, W.M., Goldfarb, R., Yin, Q.Z., 2012. Geochemical constraints on adakites of different origins and copper mineralization. J. Geol. 120, 105–120.
Sun, D.Y., Gou, J., Wang, T.H., Ren, Y.S., Liu, Y.J., Guo, H.Y., Liu, X.M., Hu, Z.C., 2013. Geochronological and geochemical constraints on the Erguna massif basement, NE China-subduction history of the Mongol–Okhotsk oceanic crust. Int. Geol. Rev. 55, 1801–1816.
Sun, X.L., Sun, W.D., Hu, Y.B., Ding, W., Ireland, T., Zhan, M.Z., Liu, J.Q., Ling, M.X., Ding, X., Zhang, Z.F., Fan, W.M., 2018. Major Miocene geological events in southern Tibet and eastern Asia induced by the subduction of the Ninetyeast Ridge. Acta Geochimica 37, 395–401.
Sylvester, P.J., 1998. Post-collisional strongly peraluminous granites. Lithos 45, 29–44.
Tang, J., Xu, W.L., Wang, F., Wang, W., Xu, M.J., Zhang, Y.H., 2014. Geochronology and geochemistry of Early-Middle Triassic magmatism in the Erguna Massif, NE China: constraints on the tectonic evolution of the Mongol-Okhotsk Ocean. Lithos 184, 1–16.
Tong, Y., Jahn, B.M., Wang, T., Hong, D.W., Smith, E.I., Sun, M., Gao, J.F., Yang, Q.D., Huang, W., 2015. Permian alkaline granites in the Erenhot–Hegenshan belt, northern Inner Mongolia, China: Model of generation, time of emplacement and regional tectonic significance. J. Asian Earth Sci. 97, 320–336.
Wang, Q., Xu, J.F., Jian, P., Bao, Z.W., Zhao, Z.H., Li, C.F., Xiong, X.L., Ma, J.L., 2006. Petrogenesis of adakitic porphyries in an extensional tectonic setting, Dexing, South China: implications for the genesis of porphyry copper mineralization. J. Petrol. 47, 119–144.
Wang, F., Xu, W.L., Xing, K.C., Tang, J., Wang, Z.W., Sun, C.Y., Wu, W., 2019. Temporal changes in the subduction of the Paleo-Pacific plate beneath Eurasia during the late Mesozoic: Geochronological and geochemical evidence from Cretaceous volcanic rocks in eastern NE China. Lithos 326-327, 415–434.
Whalen, J.B., Currie, K.L., Chappell, B.W., 1987. A-type granites: geochemical characteristics, discrimination and petrogenesis. Contrib. Mineral. Petrol. 95, 407–419.
Wu, F.Y., Sun, D.Y., Li, H.M., Jahn, B., Wilde, S., 2002. A-type granites in northeastern China: age and geochemical constraints on their petrogenesis. Chem. Geol. 187, 143–173.
Wu, F.Y., Zhao, G.C., Sun, D.Y., Wilde, S.A., Yang, J.H., 2007. The Hulan Group: its role in the evolution of the Central Asian Orogenic Belt of NE China. J. Asian Earth Sci. 30, 542–556.
Wu, F.Y., Sun, D.Y., Ge, W.C., Zhang, Y.B., Grant, M.L., Wilde, S.A., Jahn, B.M., 2011. Geochronology of the Phanerozoic granitoids in northeastern China. J. Asian Earth Sci. 41, 1–30.
Wu, F.Y., Liu, X.C., Ji, W.Q., Wang, J.M., Yang, L., 2017. Highly fractionated granites: recognition and research. Sci. China Earth Sci. 60, 1201–1219.
Wu, Q., Feng, C.Y., Qu, H.Y., Zhong, S.H., Liu, J.N., Zhang, M.Y., 2019. Geochronology, geochemistry and Hf isotopes of the Early Ordovician A-type granite in the Mohe Region, northeastern Da Hinggan mountains. Acta Geol. Sin. 93 (2), 368–380 (in Chinese with English abstract).
Xiao, W.J., Windley, B.F., Sun, S., Li, J.L., Huang, B.C., Han, C.M., Yuan, C., Sun, M., Chen, H.L., 2015. A tale of amalgamation of three Permo-Triassic collage systems in Central Asia: oroclines, sutures, and terminal accretion. Annu. Rev. Earth Planet. Sci. 43, 477–507.
Xu, B., Charvet, J., Zhang, F.Q., 2001. Primary study on petrology and geochronology of blue schist in Sunitezuoqi, northern Inner Mongolia. Chin. J. Geol. 36 (4), 424–434 (in Chinese with English abstract).
Xu, W.L., Pei, F.P., Wang, F., Meng, E., Ji, W.Q., Yang, D.B., Wei, W., 2013. Spatial-temporal relationships of Mesozoic volcanic rocks in NE China: constraints on tectonic overprinting and transformations between multiple tectonic regimes. J. Asian Earth Sci. 74, 167–193.
Xu, B., Zhao, P., Wang, Y.Y., Liao, W., Luo, Z.W., Bao, Q.Z., Zhou, Y.H., 2015. The pre-Devonian tectonic framework of Xing'an-Mongolia orogenic belt (XMOB) in North China. J. Asian Earth Sci. 97, 183–196.
Yang, J.H., Wu, F.Y., Shao, J., Simon, A.W., Xie, L.W., Liu, X.M., 2006. Constraints on the timing of uplift of the Yanshan Fold and Thrust Belt, North China. Earth Planet. Sci. Lett. 246, 336–352.
Yang, Y.C., Han, S.J., Sun, D.Y., Guo, J., Zhang, S.J., 2012. Geological and geochemical features and geochronology of porphyry molybdenum deposits in the Lesser Xing'an Range–Zhangguangcai Range metallogenic belt. Acta Petrol. Sin. 28, 379–390 (in Chinese with English abstract).
Yogodzinski, G.M., Kay, R.W., Volynets, O.N., Koloskov, A.V., Kay, S.M., 1995. Magnesian andesite in the western Aleutian Komandorsky region: implications for slab melting and processes in the mantle wedge. Geol. Soc. Am. Bull. 107, 505–519.
Zhang, F.Q., Chen, H.L., Yu, X., Dong, C.W., Yang, S.F., Pang, Y.M., Batt, G.E., 2011. Early Cretaceous volcanism in the northern Songliao Basin, NE China, and its geodynamic implication. Gondwana Res. 19, 163–176.
Zhang, L., Lv, X.B., Liu, G., Chen, J., Chen, C., Gao, Q., Liu, H., 2013. Characteristics and genesis of continental back-arc A-type granites in the eastern segment of the Inner Mongolia-Da Hinggan Mountains Orogenic belt. Geol. China 40 (3), 869–884 (in Chinese with English abstract).
Zhang, X.H., Yuan, L.L., Xue, F.H., Yan, X., Mao, Q., 2015. Early Permian A-type granites from Central Inner Mongolia, North China: magmatic tracer of postcollisional tectonics and oceanic crustal recycling. Gondwana Res. 28, 311–327.
Zhao, Z., Chi, X.G., Pan, S.Y., Liu, J.F., Sun, W., Hu, Z.C., 2010. Zircon U-Pb LA-ICP-MS dating of Carboniferous volcanic and its geological significance in the northwestern Lesser Xing' an Range. Acta Petrol. Sin. 26 (8), 2452–2464 (in Chinese with English abstract).
Zhao, Y.S., Yang, L.Q., Chen, Y.F., Qing, M., Yan, J.P., Ge, L.S., Guo, X.D., Wang, J.R., 2012. Geochemistry and zircon U-Pb geochronology of diorite porphyry associated with the Jinchang Cu-Au deposit, Heilongjiang Province. Acta Petrol. Sin. 28, 451–467 (in Chinese with English abstract).
Zhao, Y.D., Zhao, J., Wang, K.L., Che, J.Y., Wu, D.T., Xu, F.M., Li, S.C., 2013. Characteristics of the Late Carboniferious post-orogenic Dayinhe intrusion in the northwest of the Xiao Hinggan Mountains and their geological implications. Acta Petrol. Mineral. 32, 63–72 (in Chinese with English abstract).
Zhou, J.B., Wilde, S.A., 2013. The crustal accretion history and tectonic evolution of the NE China segment of the Central Asian Orogenic Belt. Gondwana Res. 23, 1365–1377.
Zhou, C.Y., Wu, F.Y., Ge, W.C., Sun, D.Y., Abdel Rahman, A.A., Zhang, J.H., Cheng, R.Y., 2005. Age, geochemistry and petrogenesis of the cumulate gabbro in Tahe, northern Da Hinggan Mountain. Acta Petrol. Sin. 21 (3), 763–775 (in Chinese with English abstract).
Zhou, J.B., Wilde, S.A., Zhao, G.C., Han, J., 2018. Nature and assembly of microcontinental blocks within the Paleo-Asian Ocean. Earth Sci. Rev. 186, 76–93.